PNAS RESEARCH ARTICLE | BIOCHEMISTRY

Structure and mechanism for iterative amide *N*-methylation in the biosynthesis of channel-forming peptide cytotoxins

Dillon P. Cogan[a], Agneya Bhushan[b], Reyvin Reyes[a], Lingyang Zhu[c], Jörn Piel[b], and Satish K. Nair[a,d,e,1]

Edited by Michael Marletta, University of California, Berkeley, CA; received September 8, 2021; accepted February 10, 2022

The polytheonamides are highly modified and potent, cytotoxic peptides with a unique β-helical structure (helical diameter ∼4 Å) that affords selective membrane permeation of monovalent cations. Toxicity has been linked to promiscuous ion-channel behavior in studies of the prototypical polytheonamide B. Specific structural features of the β-helical toxins include, among other modifications, *C*α-epimerizations and *N*γ-methylations, which have been highlighted as the early-stage modifications most critical for β-helix formation. Here, we interrogate *C*α-epimerization and *N*γ-methylation to understand the importance of these modifications for secondary structure. We characterize the mechanism of *N*γ-methylations on the amide side chains of D-Asn, an enzymatic modification with little biochemical precedent. Crystal structures of the AerE methyltransferase in complex with its epimerized peptide substrate and *S*-adenosyl-homocysteine reveal features of substrate recognition and an unexpected metal-ion that may mediate methyl transfer to the poorly nucleophilic amide. These studies provide a framework for the engineering of novel β-helical peptides with ion and membrane selectivity.

RiPP peptide | biosynthesis | natural products

Significance

The channel-forming proteusins are bacterial helical peptides that allow permeation of positively charged ions to influence membrane potential and cellular physiology. We biochemically characterize the effect of two critical posttranslational modifications on the secondary structure of the peptide substrate. We determine how a methyl group can be added to the side chains of D-Asn residues in a peptide substrate and show how flanking residues influence selectivity. These studies should foster the development of small-molecule peptide ion channels as therapeutics.

The prototypical proteusin polytheonamide B (pTB), isolated from the marine sponge *Theonella swinhoei* Y and produced by one of its uncultivated bacterial symbionts, is a member of the ribosomally synthesized and posttranslationally modified peptide (RiPP) class of natural products (1). pTB is among the most highly posttranslationally modified peptides known but requires only seven enzymes to carry out the 48 posttranslational modifications (PTMs) found in the final product (2–6). These modifications include 18 *C*α-epimerizations, 4 *C*β-hydroxylations, 17 *C*-methylations, 1 dehydration, and 8 *N*γ-methylations, which collectively transform a linear 49-residue core peptide into a bioactive β-helical structure with alternating D- and L-configured amino acids (7).

The wide-bore (0.4 nm) of the pTB helix has been shown to facilitate ion passage of monovalent cations (e.g., H^+, Na^+, and K^+) by insertion into planar bilayers, suggesting a toxification strategy by disruption of membrane potentials (4). Administration of fluorescently labeled pTB to mammalian cells revealed a two-pronged mechanism whereby membrane insertion is accompanied by membrane depolarization and endocytic internalization (8). Notably, pTB localizes to lysosomes inside MCF-7 human breast cancer cells and neutralizes the pH gradient necessary for cellular homeostasis, highlighting the utility of pTB as a lead scaffold for its development as a novel anticancer agent.

We recently characterized a new proteusin, aeronamide A, isolated from the bacterium *Microvirgula aerodenitrificans* DSM 15089 using a "tagged-bait" approach in which the *Microvirgula* host was used to generate suitable quantities of various hypermodified peptides (9). Aeronamide A disrupts membrane potential in artificial liposomes but has a simpler structure compared to pTB (35 vs. 48 PTMs). Presumably, aeronamide A also adopts a β-helical structure and inserts into membrane bilayers to function as an ion-channel.

The PTMs in aeronamide A include 21 *C*α-epimerizations, 7 *C*-methylations, 5 D-Asn *N*γ-methylations, and dehydration of the N-terminal Thr en route to the installation of a 2-ketobutyryl moiety (Fig. 1*A*). The final product, aeronamide A, lacks the *C*β-hydroxylations observed in pTB. Candidate enzymes in the aeronamide biosynthetic gene cluster that carry out these modifications were identified based on sequence similarity to the pTB machinery and consist of a radical *S*-adenosyl methionine (SAM)-dependent epimerase (AerD), a coenzyme B12-dependent radical SAM *C*-methyltransferase (AerC), a SAM-dependent *N*-methyltransferase (AerE), a LanM-like Ser/Thr dehydratase (AerF), and a serine protease (AerH) (Fig. 1 *A*–*C*). In vitro studies of pTB biosynthesis demonstrated that only epimerized PoyA peptide is the substrate for full eightfold *N*γ-methylation catalyzed by PoyE and *N*-methylation efficiency correlates with extent of epimerization (7).

Author affiliations: [a]Department of Biochemistry, University of Illinois at Urbana–Champaign, Urbana, IL 61801; [b]Institute of Microbiology, Eidgenössische Technische Hochschule Zurich, CH-8093 Zurich, Switzerland; [c]School of Chemical Sciences NMR Laboratory, University of Illinois at Urbana–Champaign, Urbana, IL 61801; [d]Center for Biophysics and Computational Biology, University of Illinois at Urbana–Champaign, Urbana IL 61801; and [e]Carl R. Woese Institute for Genomic Biology, University of Illinois at Urbana–Champaign, Urbana, IL 61801

Author contributions: D.P.C., J.P., and S.K.N. designed research; D.P.C., R.R., L.Z., and S.K.N. performed research; A.B. and R.R. contributed new reagents/analytic tools; S.K.N. analyzed data; and D.P.C., L.Z., J.P., and S.K.N. wrote the paper.

The authors declare no competing interest.

This article is a PNAS Direct Submission.

[1]To whom correspondence may be addressed. Email: snair@illinois.edu.

This article contains supporting information online at http://www.pnas.org/lookup/suppl/doi:10.1073/pnas.2116578119/-/DCSupplemental.

Published March 22, 2022.

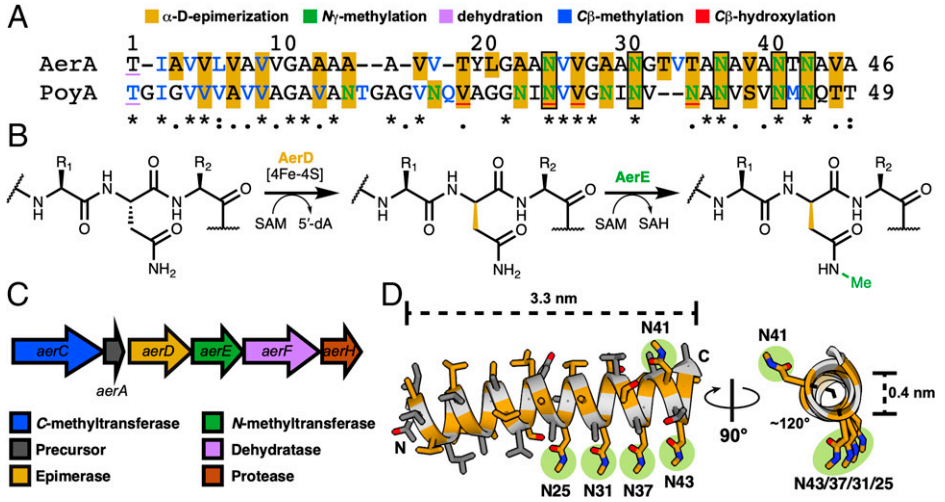

Fig. 1. Core peptide alignment, AerD/AerE-catalyzed modifications, aeronamide biosynthetic gene cluster, and β-helical model of aeronamide. (*A*) AerA/PoyA core peptide alignments with color-coded residue modifications. The five D-Asn residues methylated in AerA are fully conserved and boxed in black. (*B*) Reaction scheme depicting the unidirectional α-epimerizations installed by the radical SAM-dependent, [4Fe-4S]-containing epimerase, AerD, and D-Asn N_γ-methylations catalyzed by SAM-dependent *N*-methyltransferase, AerE (R_1 = Ala or Thr side chains; R_2 = Val, Ala, Thr, or Gly [H] side chains). (*C*) Aeronamide biosynthetic gene cluster. (*D*) Two, 90°-related, orientations of a model of β-helical AerA (preaeronamide) containing α-epimerizations and N_γ-methylations. In the absence of lipids or the membrane bilayer, the modified peptide is demonstrated to be unstructured.

Little is currently known about the timing of the modifications that establish β-helicity during proteusin maturation, as well as the minimal set of PTMs that are sufficient for ion-channel activity. Molecular dynamics simulations point to the importance of D-Asn *N*γ-methylations in maintaining the coaxial hydrogen-bond network after PTMs were systematically removed from pTB and hypothetical precursors were evaluated for their stability in silico (10). A simplistic model would suggest that the helical nature of the substrate may guide recognition by the *N*-methyltransferase, but details of substrate specificity have yet to be determined (Fig. 1*D*). Additionally, there are limited precedents of characterized enzymes that carry out the direct methylation of amide nitrogen atoms in natural products, such as those found in gliotoxin (11), ansamitocin (12), welwitindolindones (13), and omphalotins (14, 15). Detailed biochemical characterization has only been carried out on the omphalotins, in which peptide backbone amides are modified by a single-chain enzyme–substrate fusion that is unrelated to the *N*-methyltransferases involved in proteusin biosynthesis (16, 17).

Here, we characterize the mechanism of AerE-catalyzed iterative *N*-methylation of five D-Asn residues in the aeronamide core peptide. We provide evidence for a SAM-dependent and Lewis acid-mediated methylation strategy that invokes a catalytic Tyr-Asp pair and metal ion to coordinate the methylation at the γ-nitrogen of D-Asn side chains. Guided by cocrystal structures of AerE in complex with an epimerized AerA substrate, our data demonstrate that substrate recognition is guided by local sequence rather than tertiary structure and that the epimerized and methylated peptide is largely unstructured. Our biochemical and biophysical characterization inform on the requisite chemical features for bioactivity, which is critical for the design and semisyntheses of proteusin analogs with tailored membrane selectivity.

Results

In Vitro Fivefold *N*-Methylation of the AerE Substrate. We carried out in vitro reconstitution of the aeronamide A pathway by coexpressing the His_6-tagged AerA substrate in *Escherichia coli* with the radical SAM epimerase AerD to yield the epimerized AerA product ($AerA_{DL}$) (9). The AerE methyltransferase was expressed in *E. coli* as a SUMO fusion-protein and purified to homogeneity as a tag-free monomer. Incubation of AerE with $AerA_{DL}$ in the presence of SAM followed by tryptic removal of the leader peptide resulted in a +70-Da mass shift in the core peptide-containing fragment by matrix-assisted laser desorption/ionization time-of-flight mass spectrometry (MALDI-TOF MS), suggesting that AerE carries out fivefold methylation on the peptide substrate (Fig. 2 *A* and *B*). To confirm that the five D-Asn residues are the sites of methylation, we utilized tandem electrospray-ionization MS (ESI-MS/MS) to mass fingerprint the methylated $AerA_{DL}$ product (5Me-$AerA_{DL}$), as described previously, demonstrating that AerA is a D-Asn *N*γ-methyltransferase (9).

AerA *N*-Methylation Is Independent of the Leader Peptide and Requires only a Partial Core. Treatment of $AerA_{DL}$ with trypsin afforded a truncated peptide that retained the entire core peptide along with 21 of 100 residues of the leader peptide ($AerA_{DL,21LP}$) (*SI Appendix*, Fig. S1). To investigate the importance of the N-terminal 79 residues in the leader sequence, we purified the tryptic $AerA_{DL,21LP}$ product by high-performance liquid chromatography (HPLC). Treatment of $AerA_{DL,21LP}$ with AerE and SAM also resulted in complete fivefold *N*-methylation as determined by MALDI-TOF MS (*SI Appendix*, Fig. S1), demonstrating partial leader-peptide independence of AerE. To further delineate a minimal substrate of AerE, we carried out proteinase K digestion of $AerA_{DL}$ (7). HPLC purification of the proteinase K-treated peptide provided a panel of $AerA_{DL}$ core fragments that contained between 31 and 35 residues of the 46-residue core. Importantly, these fragments harbored all five D-Asn methyl-acceptors (Fig. 2*A*). Because of the difficulty in separating these fragments by reversed-phase HPLC with C4/C18 resins, we incubated the coeluted mixture of HPLC-purified peptides with AerE and SAM. Overnight incubation gave +70.2-Da mass shifts for all five species, revealing that AerE *N*-methylation occurs independent of the leader peptide and requires only a portion (≤31 residues) of its $AerA_{DL}$ core fragment (Fig. 2*C* and *SI Appendix*, Fig. S2).

We previously measured the D-residue content of epimerized PoyA using advanced Marfey's analysis and observed that complete epimerization by PoyD requires multiple days of

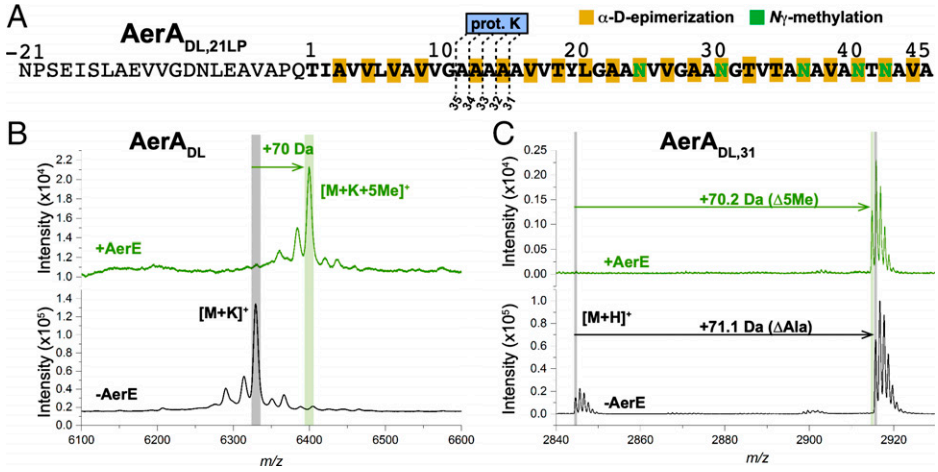

Fig. 2. Minimal substrate requirement of AerE-catalyzed *N*-methylation. (*A*) Sequence representation of $AerA_{DL,21LP}$ with core peptide residues in bold and sites of proteinase K cleavage marked with dashed lines. (*B*) $AerA_{DL}$ treated with (green) or without (black) AerE confirms the AerE-dependent +70-Da mass shift consistent with penta-*N*-methylation. (*C*) The shortest proteinase K fragment, $AerA_{DL,31}$, isolated by HPLC is similarly penta-*N*-methylated in the presence of AerE (green). Note, the +71.1-Da shift in the AerE reaction corresponds to the desmethylated 32mer proteinase K fragment, $AerA_{DL,32}$, which differs from $AerA_{DL,31}$ by one Ala residue.

coexpression in *E. coli* (7). Our in vivo preparation of epimerized AerA was purified after a comparatively shorter coexpression with the aeronamide epimerase AerD (~1 d). Thus, we wondered whether incomplete epimerization of AerA might have influenced the in vitro AerE-catalyzed *N*-methylation reactions. To resolve this uncertainty, we chemically synthesized a truncated 34mer fragment corresponding to the C terminus of the epimerized AerA core peptide ($AerA_{DL,34}$) by solid-phase peptide synthesis (SPPS), thereby ensuring that all appropriate D-residues were in place. To probe whether L-Asn can also be methylated by AerE, we used the same SPPS approach to synthesize an otherwise identical peptide comprised of all L-residues ($AerA_{L,34}$). Whereas complete fivefold *N*-methylation by AerE was observed after 25 h for the epimerized peptide $AerA_{DL,34}$, no detectable methylations of $AerA_{L,34}$ were observed (*SI Appendix*, Fig. S3). These studies conclusively demonstrate that the leader peptide is not required for *N*γ-methylation and that this modification is only installed on epimerized D-Asn residues.

Timing and Directionality of AerE D-Asn *N*γ-Methylation. The progress of D-Asn *N*γ-methylation was probed by heat-precipitating the enzyme at various time points between 0 and 16.5 h and quantifying relative peak intensities of methylated $AerA_{DL}$ intermediates by MALDI-TOF MS. Comparing the normalized peak intensities of mono- through penta-*N*γ-methylated $AerA_{DL}$ is indicative of a time-dependent loss in processivity of AerE, as more extensively methylated $AerA_{DL}$ intermediates appear to have longer lifetimes (Fig. 3*A*). Given the time-dependent relative populations of mono- through penta-*N*γ-methylated $AerA_{DL}$ (1Me–5Me), we isolated the 1Me–4Me intermediates by heat-quenching and tryptic digesting the reactions at various time points in order to study the directionality of AerE by ESI-MS/MS.

In the case of 1Me, we predominantly observed y-ions with no mono-*N*γ-methylation beyond D-Asn25 and only two y-ions (y19+Me/y19-NH_3+Me) with methylation of a fragment born of cleavage between D-Asn25 and D-Asn31, suggesting that D-Asn25 and D-Asn31 are early methyl acceptors (Fig. 3*B* and *SI Appendix*, Figs. S4 and S5 and Table S3). Fragmentation of 2Me and 3Me revealed a lack of regioselectivity with respect to D-Asn31, D-Asn37, and D-Asn41 for the second and third methylation events (Fig. 3*B* and *SI Appendix*, Figs. S4 and S5 and Tables S4 and S5). Importantly, the y5+Me ion, corresponding to methylation at D-Asn43, was only observed in the 3Me and 4Me species, suggesting it is the slowest to be methylated (Fig. 3*B* and *SI Appendix*, Figs. S4 and S5 and Tables S5 and S6).

To reconcile the observed pseudo(*N*-to-*C*)-directionality of AerE, we built a β-helical model of the AerA core peptide based on the pTB solution NMR structure (Fig. 1*D*) (4). Inspection of the model reveals that D-Asn25, D-Asn31, D-Asn37, and D-Asn43 are situated on the same face of the β-helix, whereas D-Asn41 is separated by ~120° about the helical axis, despite it being methylated faster (on average) than D-Asn43 (Figs. 1*D* and 3*B* and *SI Appendix*, Figs. S4 and S5 and Tables S1–S6). The discordance between residue position and observed rates of *N*γ-methylation hinted that D-Asn recognition might be more dependent on local residue environment rather than its positional context within a β-helical structure. If the β-helical structure influenced accessibility of D-Asn to AerE, then all D-Asn residues on the same face (i.e., D-Asn25, D-Asn31, D-Asn37, and D-Asn43) would likely be *N*γ-methylated before D-Asn41, but our data demonstrate that this was not the case.

Epimerized and *N*-Methylated $AerA_{DL,34}$ Is Unstructured and Not *β*-Helical. To further test the notion that AerE operates on an unstructured peptide throughout iterative *N*-methylation, we studied the solution NMR structures of $AerA_{DL}$ containing or lacking all five D-Asn *N*γ-methylations. We synthesized the desmethylated $AerA_{DL,34}$ from commercially available building blocks ($AerA_{DL,34}$) using the same synthetic SPPS strategy described above. A 34-residue fragment containing all five D-Asn *N*γ-methylations (5Me-$AerA_{DL,34}$) was synthesized by adapting methods from Itoh et al. (18), to yield an acid-labile, side chain-protected precursor to the noncanonical *N*γ-Me-D-Asn residue (compound **6** in *SI Appendix*, Scheme S1 and Figs. S6–S10). Global deprotection and HPLC purification of the SPPS-derived peptides yielded sufficient quantities (≥3 mg) to carry out detailed NMR analyses (*SI Appendix*, Fig. S11).

Initially, we attempted to study the peptides under solvent conditions that were previously used to characterize the β-helical pTB (i.e., 1:1 [vol/vol], $CDCl_3/CD_3OH$) (4); however, significant peak broadening observed in the ^{1}H-NMR

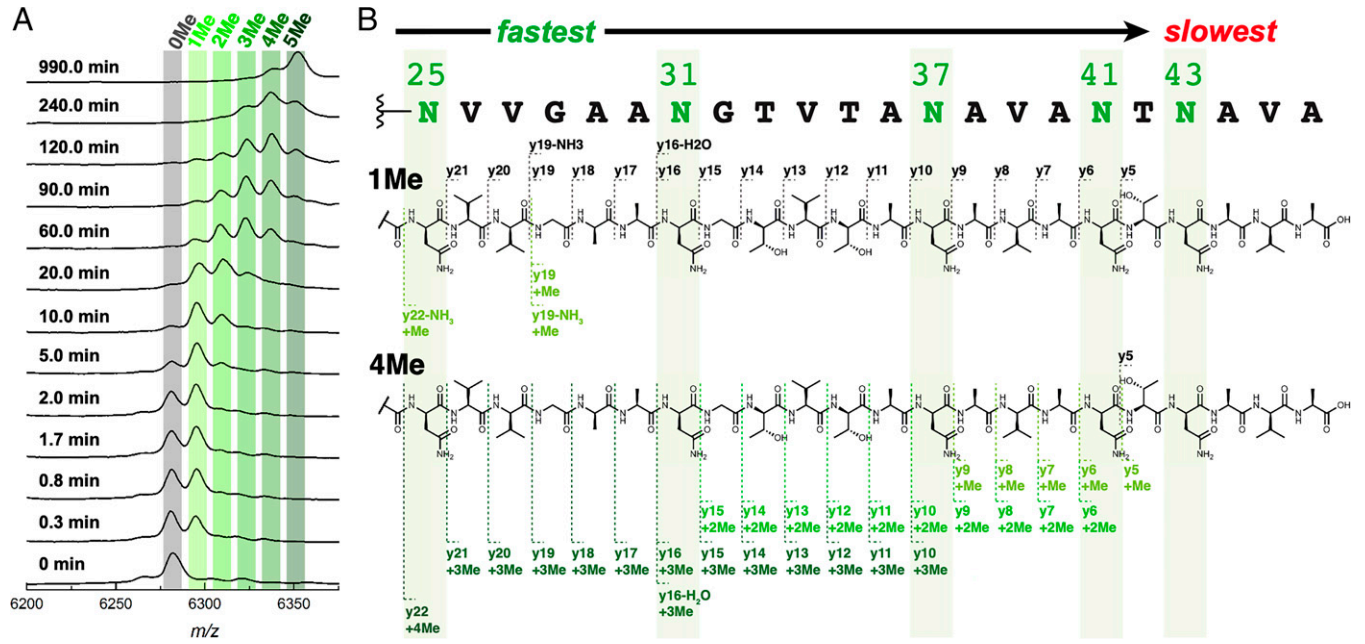

Fig. 3. Processivity and pseudo(*N*-to-*C*)-directionality of AerE-catalyzed *N*-methylation analyzed by ESI-MS/MS. (*A*) Time course of penta-*N*-methylation of $AerA_{DL}$ by AerE (0Me → 5Me) represented as normalized MALDI-TOF MS mass intensities. AerE processivity appears to diminish as the substrate becomes more methylated. (*B*) ESI-MS/MS fragmentation analysis for the HPLC-purified mono- and tetra-*N*-methylated $AerA_{DL}$ intermediates (1Me and 4Me; for the full set of 0Me – 4Me analyses, see in *SI Appendix*, Figs. S4 and S5). Observed y-ions with no methylation are demarcated above the peptide in black dotted lines, whereas methylated intermediates are below the peptide in green (observed and calculated masses along with mass errors are tabulated in *SI Appendix*, Tables S2–S6).

spectra prevented further analysis. Conversely, CD_3OH spiked with ∼7% H_2O gave rise to clearly resolved peaks in the NH and aliphatic regions in the ^{1}H-NMR spectra for both peptides and was therefore selected for subsequent NMR experiments. (We note that these solvent conditions do not adequately simulate the membrane environment, in which the modified peptides may adopt different secondary structures. Nonetheless, they provide an assessment of the structural features recognized by AerE in solution.) Each ^{1}H-NMR spectrum harbored a cluster of NH peaks confined to ∼7.8 to 8.7 ppm, hinting at a comparably low degree of secondary structure (*SI Appendix*, Figs. S12 and S13).

Two-dimensional (2D) TOCSY and NOESY NMR spectra were collected to aid in residue peak assignments, from which all peaks could be assigned to their particular residue types (*SI Appendix*, Figs. S14–S25). Significant peak overlap led to a number of ambiguities in the sequential residue assignments because of high residue redundancy in the peptide sequences. Nonetheless, information on peptide secondary structure could be gleaned from partial residue assignments and the 2D NOESY spectra (*SI Appendix*, Figs. S16–S25). Whereas NOE sequential $d_{N(\alpha,\beta,\gamma)}(i, i-1)$ cross-peaks between residues were observed in both cases, no higher-order $d_{N(\alpha,\beta,\gamma)}(i, i-3$ or $i, i \pm 6)$ cross-peaks could be detected in either case, which would be indicative of α- or β-helical structure (Fig. 4 and *SI Appendix*, Figs. S18–S25 and Tables S7–S9). Together, our ESI-MS/MS and NMR data support the idea that an epimerized AerA core fragment bearing the five D-Asn substrates of AerE is predominantly unstructured in solution and that full penta-*N*-methylation does not promote the formation of a β-helix in a polar protic environment. Hence, AerE driven *N*-methylation is likely to be independent of secondary structure in the peptide substrate.

Crystal Structure of AerE and Cocrystal Complex with a Minimal Substrate AerA Peptide. In order to delineate the mechanism for D-Asn *N*γ-methylation, we determined the crystal structure of AerE in complex with *S*-adenosyl homocysteine (SAH) to 1.51 Å resolution (Fig. 5*A*). Overall, AerE contains a core α/β Rossmann fold seen in other class I SAM-dependent *N*-methyltransferases, such as GenN (PDB ID code 5U18; Dali *z*-score of 24.9, root mean square deviation [RMSD] of 2.8 Å over 274 aligned Cα atoms) and PrmC (formerly HemK; PDB ID code 2B3T; Dali *z*-score of 17.9, RMSD of 3.9 Å over 216 aligned Cα atoms) (19). The former catalyzes *N*-methylation of a secondary amine in biosynthesis of the aminoglycoside gentamycin (20), while the latter *N*5-methylates a Gln within a tripeptide motif (GGQ) of prokaryotic translation termination release factors (RF1 and RF2) (21, 22). A superposition of each of these structures with AerE reveals two insertions in AerE (Gln23–Arg60 and Ala315–Leu350) (Fig. 5*A* and *SI Appendix*, Fig. S26). Features of the SAM binding C-terminal Rossmann subdomain (Ile138–Ser316) are well aligned, whereas the primarily α-helical N-terminal subdomain (Met1–Glu131) only partially aligns with GenN and is highly divergent with respect to PrmC. In PrmC, this α-helical N-terminal region employs 13 residues (of 29) to make protein–protein contacts with its methyl-acceptor substrate RF1 (22). In the case of GenN, it was proposed that the N-terminal domain interfaces with other enzymes in the gentamycin biosynthetic gene cluster (20).

To better understand the basis for substrate recognition by AerE, we also solved the 1.71 Å resolution cocrystal structure of AerE bound to $AerA_{DL,34}$, and SAH (Fig. 5 *B* and *C*). Global comparison of the substrate-free AerE structure suggests that peptide binding does not cause significant reorganization of the enzyme (RMSD of 0.15 Å over 2,561 atoms, which is 87% of the nonhydrogen atoms). Consistent with the above data, the peptide binds in an extended and unstructured configuration. Electron density corresponding to D-Thr19–Gly28 (representing 10 of the 34 residues of the $AerA_{DL,34}$ substrate) is visible in the structure (Fig. 5*B*). Unambiguous electron density for D-Asn25 is adjacent to the SAH, in agreement with the

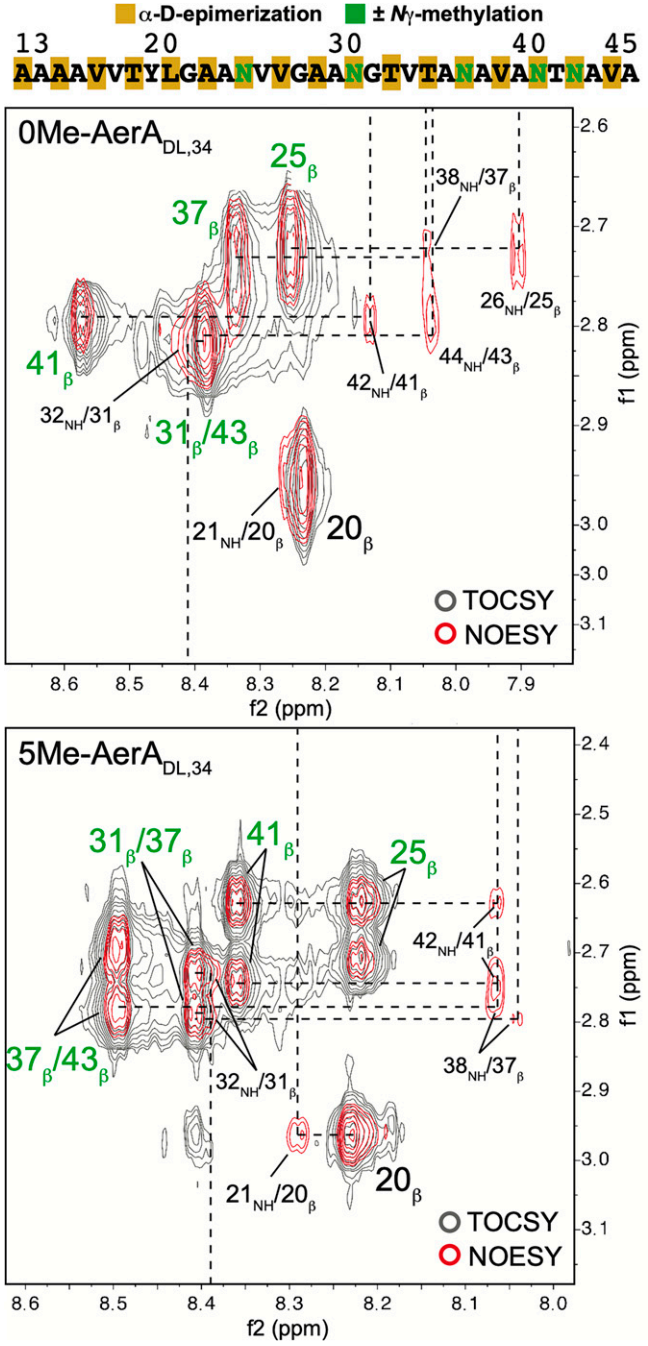

Fig. 4. Solution NMR analysis of a synthetic, epimerized AerA core peptide lacking or containing *N*-methylations. Representative regions of the 2D TOCSY and NOESY NMR spectra corresponding to the correlated NH- and β-proton chemical shifts for D-Asn or *N*γ-Me-D-Asn present in 0Me-$AerA_{DL,34}$ or 5Me-$AerA_{DL,34}$, respectively. Both peptides were synthesized by SPPS (*SI Appendix*, Fig. S11). Due to peak overlap, some of the residue assignments are ambiguous. Nonetheless, NOE $d_{N(\alpha,\beta,\gamma)}(i, i-3 \text{ or } i, i \pm 6)$ cross-peaks were not detected between any of the D-Asn or *N*γ-Me-D-Asn residues in either peptide (*SI Appendix*, Figs. S18–S25 and Tables S7–S9).

ESI-MS/MS data supporting that this residue is an early methyl acceptor (Fig. 3*B* and *SI Appendix*, Figs. S4 and S5 and Tables S2–S6).

In the active site, the γ-nitrogen of D-Asn25 is 3.7 Å away from the sulfur of SAH, where it would be directly poised for nucleophilic attack of the SAM methyl group (Fig. 5 *B* and *C*). However, the sp^2-hybridized amide nitrogen atom, whose lone pair of electrons is delocalized with the carbonyl, would not be a particularly good nucleophile. Generation of the more nucleophilic amidate would require either a strong base, twisting of the resonance plane, or a catalytically requisite metal. Inspection of the difference Fourier map ($F_{obs} - F_{calc}$) revealed density consistent with a heavy atom adjacent to the D-Asn25 amide. Presumably, the metal acts via a Lewis acid-type activation, whereby coordination of the amide oxygen might lower the rotational barrier of the amide C–N bond; thus, liberating the lone pair electrons for increased nucleophilicity. We attempted to determine if the metal ion was essential by incubating AerE with an excess of EDTA or EGTA accompanied by overnight dialysis. Surprisingly, AerE was still able to carry out penta-*N*-methylation of $AerA_{DL,34}$ after prolonged incubation, perhaps hinting that a monovalent ion (i.e., Na^+ or K^+) may be involved in catalysis, as these were present at relatively high concentrations in the buffer (*SI Appendix*, *Materials and Methods* and Fig. S27). Factoring in ideal metal–ligand bond lengths and coordination geometry (23), inspection of the $F_{obs} - F_{calc}$ maps was most consistent with an octahedrally coordinated Na^+ ion (*SI Appendix*, Fig. S28). Therefore, we have putatively assigned Na^+ as the structurally and catalytically relevant ion, which is also consistent with the inability of EDTA/EGTA to modulate activity. (For a note on Zn^{2+}-induced inhibition of AerE, see *SI Appendix*, Fig. S29.)

Examination of the ternary complex structure of AerE/$AerA_{DL,34}$/SAH also offers a plausible explanation for the slower kinetics of methylation at D-Asn43. In the core peptide, each of the D-Asn residues is primarily flanked by amino acids with small, neutral side chains (i.e., Gly, D/L-Ala, D/L-Val, and D/L-Thr). A sequence alignment of the −2 through +2 residues surrounding five of the most conserved Asn residues in polytheonamide B, aeronamide A, and the polygenonamides A1/A2 highlights the prevalence of small, neutral side chains recognized by each of the proteusin *N*-methyltransferases and a nearly identical incidence of Asn at the +2 and −2 positions (*SI Appendix*, Fig. S30) (9). In the crystal structure, the −2 residue to D-Asn25 is a D-Ala and its side chain points into a hydrophobic surface of AerE (toward Pro321 and Ile322), whereas the +2 residue (D-Val27) is more solvent-exposed and directed away from AerE; perhaps explaining why a D-Asn is more tolerated at the +2 position. In contrast, D-Asn41 and D-Asn43 each have a relatively bulkier D-Asn in their +2 and −2 positions, respectively. Moreover, the hydrophobic nature of the binding pocket for the −2 residue would favor binding of a methylated D-Asn, in agreement with the observation that *N*γ-methylation of D-Asn41 occurs before modification at D-Asn43 (on average).

Site-Directed Mutagenesis and *N*-Methylation Activity of AerE. Based on sequence conservation and active-site proximity, we generated site-directed variants of AerE corresponding to Y137F, D141A, D141N, N231A, F234A, and V235A, and tested their *N*-methylation activities with the synthetic substrate $AerA_{DL,34}$ (Fig. 5 *B* and *C*). Following prolonged incubation of the wild-type and variant AerE with SAM and $AerA_{DL,34}$, MALDI-TOF MS analysis revealed the Y137F, D141A, D141N, N231A, and F234A variants were all nearly devoid of activity with only trace amounts of dimethylation catalyzed by variant N231A and trace amounts of monomethylation catalyzed by variants Y137F and D141A (Fig. 6*A*). The side chain of Val235 is in van der Waals contact distance from the Hα of D-Asn25, but the V235A variant retained activity and catalyzed tetramethylation of the substrate (Fig. 5*C*).

Given that the Y137F variant was catalytically inactive, we more-closely examined the interactions mediated by Tyr137.

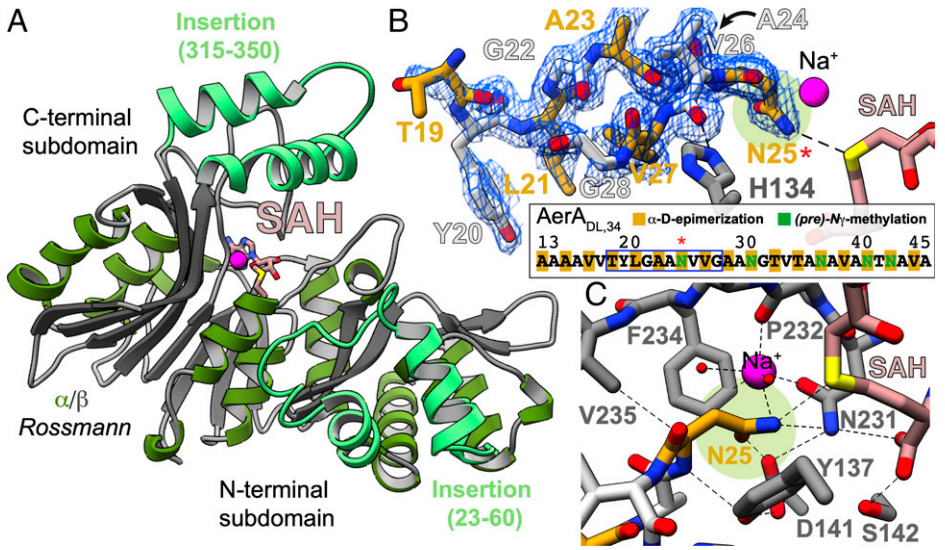

Fig. 5. Structural analysis of AerE bound to SAH and its methyl-acceptor substrate $AerA_{DL,34}$. (*A*) Overall ribbon diagram of AerE bound to SAH. (*B*) Simulated annealing difference Fourier map (F_{obs} – F_{calc}) contoured at 2σ centered around 10 residues of $AerA_{DL,34}$ visible by electron density (boxed in blue). (*C*) Close-up of the AerE active site with labeled interatomic distances (2.0 to 3.7 Å).

The phenolic group is within hydrogen-bonding distance (2.5 Å) with the side chain carboxylate of Asp141 and with the backbone amide nitrogen of D-Asn25 (3.2 Å) (Fig. 5*C*). Asp141 extends this hydrogen-bond network and is 3.1 Å away from the amide side chain of Asn231 and 2.0 Å away from the D-Asn25 side chain of $AerA_{DL,34}$ These hydrogen-bonding interactions are collectively essential for activity, given the detrimental effect of site-specific variants at any of these positions (Fig. 5*C*).

We next determined the cocrystal structures of several site-directed variants to provide a structural context of their functional significance. We first determined the structure of Y137F-AerE in complex with SAH. The structure of this variant is nearly identical to that of the wild-type enzyme and suggests that the loss of activity is due to a direct role of the Tyr137 phenolic oxygen in catalysis (*SI Appendix*, Fig. S31). The structure of the D141A-AerE/SAH complex reveals that the Tyr137 side chain moves toward SAH and disrupts the interactions with the substrate-backbone observed in the wild-type. The importance of this interaction in catalysis is reflected by the loss of activity in the D141A variant (*SI Appendix*, Fig. S31).

The structure of N231A-AerE/SAH was determined from crystals grown under identical conditions to that for the wild-type enzyme but lacks electron density corresponding to the bound Na^+ ion (*SI Appendix*, Fig. S31). In the structure of the wild-type enzyme, Asn231 coordinates with this metal ion with a separation distance of 2.5 Å. Presumably, the loss of the

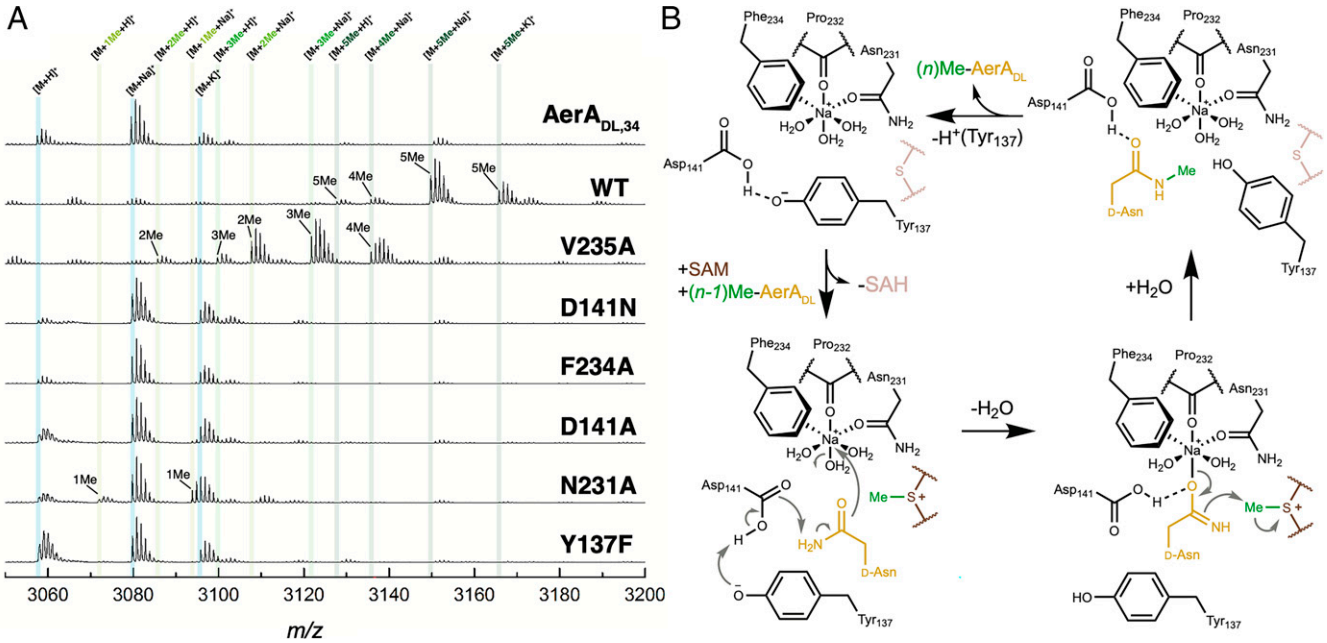

Fig. 6. Mutational analysis and proposed mechanism of AerE-catalyzed amide *N*-methylation. (*A*) Extents of $AerA_{DL,34}$ *N*-methylation by wild-type (WT) or site-directed variants of AerE were measured following end-point reactions (16 h) by MALDI-TOF MS. The top mass spectrum corresponds to an enzyme-free control reaction containing $AerA_{DL,34}$ and SAM. (*B*) Proposed catalytic cycle for AerE-catalyzed metal- (Na^+) and SAM-dependent D-Asn *N*γ-methylation (*n* = number of catalytic cycle iterations).

bound Na^+ ion in the N231A variant is a critical contributor to the loss of activity. Similarly, in the wild-type structure Phe234 provides one surface of the binding pocket for the Na^+ ion, separated by a 3.0 Å cation–π interaction, and the loss of activity in the F234A variant provides further support for this metal ion in catalysis (24–26). Catalytic activities for additional site-directed AerE variants are reported in *SI Appendix*, Fig. S32.

Discussion

Channel-forming peptide cytotoxins of the proteusin family modulate intracellular and organellar ion concentrations with membrane specificity. As such, these natural compounds present promising scaffolds for the development of anticancer and antimicrobial agents. The enzymes that assemble the peptides in nature are impressively efficient, with just three enzymes responsible for 30+ modifications (i.e., α-epimerizations and *N*- and *C*-methylations). While synthetic and highly modular routes to the proteusins have been developed, such heroic efforts are labor-intensive and require >70 steps (8, 18, 27).

As a step toward a simpler and more sustainable one-pot enzymatic synthesis, we have dissected the structural and catalytic properties of one relevant enzyme from a recently characterized proteusin, aeronamide A. Our studies of the *N*-methyltransferase AerE show that this enzyme functions independent of the substrate leader peptide and can efficiently install all five of the D-Asn *N*γ-methylations on an epimerized peptide substrate. Isolation of the intermediates en route to the penta-*N*-methylated product followed by MS/MS analysis revealed that AerE operates with pseudo(*N*-to-*C*)-directionality and that the C-terminal D-Asn43 is slowest to be methylated, despite its position on the same face of the β-helix as earlier methyl acceptors. Solution NMR analyses of epimerized AerA core peptides containing or lacking the *N*-methylations are characteristic of a predominantly unstructured peptide, supporting the notion that α-epimerizations and *N*-methylations are not sufficient to induce the β-helical structure.

Based on structural and mutational studies of AerE in complex with its peptide substrate, we suggest a plausible mechanism for metal- and SAM-assisted amide *N*-methylation. A similar mechanism for SAM/Fe-dependent *C*-methylation was previously identified in apratoxin A biosynthesis (28). Upon binding of the peptide substrate, our proposed mechanism for AerE-catalyzed *N*-methylation begins with activation of Asp141 by the phenolic side-chain of Tyr137 to deprotonate the D-Asn side chain amide. The resultant amidate is stabilized by the catalytically requisite Na^+ ion concomitant with the displacement of an axially coordinated solvent molecule. Proximity of the amidate to the SAM methyl group would facilitate transfer onto the amide nitrogen via nucleophilic attack. Rehydration of the Na^+ ion and dissociation of the *N*γ-Me-D-Asn product would reset the enzyme for binding to the next D-Asn substrate (Fig. 6*B*). Overall, our investigation into proteusin *N*-methylation provides a structural and mechanistic framework for the continued exploration of a promising class of peptide ion-channels (29).

Materials and Methods

The *SI Appendix, Materials and Methods* include methods for expression and purification for AerA substrate peptides, AerE methyltransferase, and other proteins used in this study. Methodology for peptide synthesis, activity assays, crystallization, NMR spectra, binding studies, and mutational analyses are also detailed therein.

Data Availability. The crystal structure data have been deposited in the Protein Data Bank (PDB ID codes 7RC2 [wild-type AerE bound to SAH], 7RC3 [Y173F AerE], 7RC4 [D141A AerE], 7RC5 [N231A AerE], and 7RC6 [wild-type AerE bound to modified peptide substrate]).

ACKNOWLEDGMENTS. We thank members of the S.K.N. and J.P. laboratories for constructive discussions and assistance with instrumentation, and Keith Brister, Spencer Anderson, and colleagues at Life Sciences Collaborative Access Team (Argonne National Laboratories) for facilitating X-ray data collection. This work was supported by NIH Grant GM079038 (to S.K.N.).

1. M. Montalbán-López *et al.*, New developments in RiPP discovery, enzymology and engineering. *Nat. Prod. Rep.* **38**, 130–239 (2021).
2. T. Hamada, T. Sugawara, S. Matsunaga, N. Fusetani, Polytheonamides, unprecedented highly cytotoxic polypeptides, from the marine sponge *Theonella swinhoei*: 1. Isolation and component amino acids. *Tetrahedron Lett.* **35**, 719–720 (1994).
3. T. Hamada, S. Matsunaga, G. Yano, N. Fusetani, Polytheonamides A and B, highly cytotoxic, linear polypeptides with unprecedented structural features, from the marine sponge, *Theonella swinhoei*. *J. Am. Chem. Soc.* **127**, 110–118 (2005).
4. T. Hamada *et al.*, Solution structure of polytheonamide B, a highly cytotoxic nonribosomal polypeptide from marine sponge. *J. Am. Chem. Soc.* **132**, 12941–12945 (2010).
5. M. F. Freeman *et al.*, Metagenome mining reveals polytheonamides as posttranslationally modified ribosomal peptides. *Science* **338**, 387–391 (2012).
6. M. C. Wilson *et al.*, An environmental bacterial taxon with a large and distinct metabolic repertoire. *Nature* **506**, 58–62 (2014).
7. M. F. Freeman, M. J. Helf, A. Bhushan, B. I. Morinaka, J. Piel, Seven enzymes create extraordinary molecular complexity in an uncultivated bacterium. *Nat. Chem.* **9**, 387–395 (2017).
8. A. Hayata, H. Itoh, M. Inoue, Solid-phase total synthesis and dual mechanism of action of the channel-forming 48-mer peptide polytheonamide B. *J. Am. Chem. Soc.* **140**, 10602–10611 (2018).
9. A. Bhushan, P. J. Egli, E. E. Peters, M. F. Freeman, J. Piel, Genome mining- and synthetic biology-enabled production of hypermodified peptides. *Nat. Chem.* **11**, 931–939 (2019).
10. A. Renevey, S. Riniker, The importance of N-methylations for the stability of the $\beta^{6.3}$-helical conformation of polytheonamide B. *Eur. Biophys. J.* **46**, 363–374 (2017).
11. J. D. Dutcher, J. R. Johnson, W. F. Bruce, Gliotoxin, the antibiotic principle of *Gliocladium fimbriatum*. IV. The structure of gliotoxin: The action of selenium. *J. Am. Chem. Soc.* **66**, 619–621 (1944).
12. E. Higashide *et al.*, Ansamitocin, a group of novel maytansinoid antibiotics with antitumour properties from Nocardia. *Nature* **270**, 721–722 (1977).
13. K. Stratmann *et al.*, Welwitindolinones, unusual alkaloids from the blue-green algae *Hapalosiphon welwitschii* and *Westiella intricata*. Relationship to fischerindoles and hapalinodoles. *J. Am. Chem. Soc.* **116**, 9935–9942 (1994).
14. S. Ramm *et al.*, A self-sacrificing N-methyltransferase is the precursor of the fungal natural product omphalotin. *Angew. Chem. Int. Ed. Engl.* **56**, 9994–9997 (2017).
15. N. S. van der Velden *et al.*, Autocatalytic backbone N-methylation in a family of ribosomal peptide natural products. *Nat. Chem. Biol.* **13**, 833–835 (2017).
16. H. Song *et al.*, A molecular mechanism for the enzymatic methylation of nitrogen atoms within peptide bonds. *Sci. Adv.* **4**, eaat2720 (2018).
17. C. Ongpipattanakul, S. K. Nair, Molecular basis for autocatalytic backbone N-methylation in RiPP natural product biosynthesis. *ACS Chem. Biol.* **13**, 2989–2999 (2018).
18. H. Itoh, S. Matsuoka, M. Kreir, M. Inoue, Design, synthesis and functional analysis of dansylated polytheonamide mimic: An artificial peptide ion channel. *J. Am. Chem. Soc.* **134**, 14011–14018 (2012).
19. L. Holm, P. Rosenström, Dali server: Conservation mapping in 3D. *Nucleic Acids Res.* **38**, W545–W549 (2010).
20. P. D. S. Bury *et al.*, Structural basis of the selectivity of GenN, an aminoglycoside N-methyltransferase involved in gentamicin biosynthesis. *ACS Chem. Biol.* **12**, 2779–2787 (2017).
21. H. L. Schubert, J. D. Phillips, C. P. Hill, Structures along the catalytic pathway of PrmC/HemK, an N5-glutamine AdoMet-dependent methyltransferase. *Biochemistry* **42**, 5592–5599 (2003).
22. M. Graille *et al.*, Molecular basis for bacterial class I release factor methylation by PrmC. *Mol. Cell* **20**, 917–927 (2005).
23. K. B. Handing *et al.*, Characterizing metal-binding sites in proteins with X-ray crystallography. *Nat. Protoc.* **13**, 1062–1090 (2018).
24. A. S. Mahadevi, G. N. Sastry, Cation-π interaction: Its role and relevance in chemistry, biology, and material science. *Chem. Rev.* **113**, 2100–2138 (2013).
25. C. Ruan, M. T. Rodgers, Cation-π interactions: Structures and energetics of complexation of Na+ and K+ with the aromatic amino acids, phenylalanine, tyrosine, and tryptophan. *J. Am. Chem. Soc.* **126**, 14600–14610 (2004).
26. M. R. Davis, D. A. Dougherty, Cation-π interactions: Computational analyses of the aromatic box motif and the fluorination strategy for experimental evaluation. *Phys. Chem. Chem. Phys.* **17**, 29262–29270 (2015).
27. M. Inoue *et al.*, Total synthesis of the large non-ribosomal peptide polytheonamide B. *Nat. Chem.* **2**, 280–285 (2010).
28. M. A. Skiba *et al.*, A mononuclear iron-dependent methyltransferase catalyzes initial steps in assembly of the apratoxin A polyketide starter unit. *ACS Chem. Biol.* **12**, 3039–3048 (2017).
29. D. P. Cogan, "Mechanistic interrogations of ribosomal and non-ribosomal natural product enzymes," PhD thesis, University of Illinois at Urbana–Champaign, Urbana, IL (2019).